Applied Energy Science
https://www.sciltp.com/journals/aes

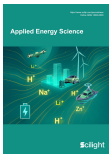

Review

From Two-Dimensional Star Materials to High-Performance Batteries: Research Status and Development Direction of MXene

Dongfang Guo [1,*] and Xu Li [1,2,*]

[1] Institute of Chemistry, Henan Academy of Sciences, Zhengzhou 450000, China
[2] Institute of Chemistry Co., Ltd., Henan Academy of Sciences, Zhengzhou 450002, China
* Correspondence: gdf970423@163.com (D.G.); lixu8218@hnas.ac.cn (X.L.)

How To Cite: Guo, D.; Li, X. From Two-Dimensional Star Materials to High-Performance Batteries: Research Status and Development Direction of MXene. *Applied Energy Science* **2026**, *1*(1), 1.

Received: 28 January 2026
Revised: 2 March 2026
Accepted: 10 March 2026
Published: 17 March 2026

Abstract: As a new type of two-dimensional (2D) transition metal carbide/nitride, MXene shows great potential in the field of electrochemical energy storage due to its high conductivity, adjustable interlayer spacing, rich surface functional groups and excellent mechanical properties. As a multifunctional electrode carrier, MXene can effectively help alleviate the volume expansion of high-capacity materials and help overcome the problems of poor conductivity, easy dissolution and structural collapse. The MXene protective layer can be used as a physical barrier to reduce the side reactions at the electrode interface and redistribute the electric field and ion flux at the interface, thereby guiding the uniform nucleation and deposition of cations. In lithium-sulfur batteries, MXene can be used as an adsorbent and catalytic conversion center for polysulfides, which significantly inhibits the side reactions caused by polysulfides. Studies have shown that the structural stability and electrochemical state of MXene can be significantly optimized through strategies such as interface engineering, interlayer regulation, and structural design. Nevertheless, MXene still faces challenges such as insufficient stability, high cost, and unclear energy storage mechanism. This paper systematically reviews the latest research progress of MXene in the field of batteries, aiming to provide useful guidance for the design of next-generation high-performance batteries.

Keywords: rechargeable batteries; MXene electrodes; electrode design; future prospects

1. Introduction

The dual challenges of energy crisis and climate change accelerate the development of renewable energy. In this major transformation from fossil fuels to renewable energy, safe, efficient and sustainable energy storage technology has become a key factor in assisting change. Rechargeable battery technology occupies a core position in many energy storage devices due to its flexibility and efficiency [1]. At present, rechargeable batteries are not only the driving power source of electric vehicles, but also an indispensable device for the smart grid to balance fluctuations and maintain the operation of portable electronic devices [2,3]. Limited by the limitations of lithium-ion batteries (LIBs) in terms of energy density, safety and resource utilization, it is particularly important to continuously explore new electrode materials to break through the shackles of existing technologies. Since the 2D transition metal carbon/nitride MXene was first reported in 2011, it has quickly attracted widespread attention due to its excellent properties. The MXene material was originally synthesized by Yury Gogotsi's team by selectively etching the A-layer atoms in the MAX phase, and then became the research focus in the field of material science and energy storage [4]. Benefiting from the exquisite surface properties of atomic arrangement, MXene exhibits extraordinary properties, including excellent electronic conductivity, easy processing, and excellent mechanical

properties comparable to metals, and its rich surface chemical sites constitute an ideal interface reaction platform (Figure 1). These characteristics bring revolutionary hope to solve the long-standing problems of battery technology, such as slow reaction kinetics, electrode volume expansion, shuttle effect and interface instability.

MXene shows extraordinary potential in LIBs [5]. Its open interlayer channels and excellent conductive network assist the electrode material to improve the Li^+ diffusion rate, and finally achieve excellent rate performance [6]. 2D MXene nanosheets can effectively combine with high-capacity alloy electrode materials such as silicon and tin, effectively buffer the structural collapse induced by material volume expansion, and construct a stable high-conductivity framework, thereby prolonging the cycle life of the electrode [7]. Interestingly, MXene can also be used as a conductive additive or coating material for lithium oxide or lithium-rich manganese cathodes, significantly improving the conductivity and structural stability of the electrode under high pressure conditions while inhibiting the decomposition of the electrolyte [8]. MXene plays a more critical role in metal-sulfur battery systems with high energy density potentials (such as Li-S and Na-S). It is well known that the 'shuttle effect' of polysulfides is the culprit for the capacity decay of metal-sulfur batteries [9]. Polysulfides are firmly anchored in the cathode region through a dual mechanism of strong chemical adsorption and physical confinement due to the polar surface of MXene and a flexible and adjustable interlayer spacing. At the same time, the extraordinary conductivity of MXene can accelerate the kinetics of sulfur redox reaction and further catalyze the reversible conversion of polysulfides. The separator material based on MXene modification has the function of efficient ion sieve, which greatly prevents the migration of polysulfides to the anode [10]. These synergistic effects together improve the cycle stability and coulombic efficiency of metal-sulfur batteries. It is worth noting that MXene is also widely used in the electrolyte of rechargeable batteries. In the liquid electrolyte system, MXene is not used as the main body of ion conduction, but as a multifunctional additive or functional carrier to adjust the ion transport behavior, stabilize the electrode interface and broaden the voltage window [11–13]. In the field of solid-state electrolytes, MXene shows more core and direct potential, mainly as a high-performance filler or functional component to synthesize composite solid-state electrolytes, eventually constructing high-speed ion channels, greatly improving mechanical strength, and inhibiting dendrites [14–17].

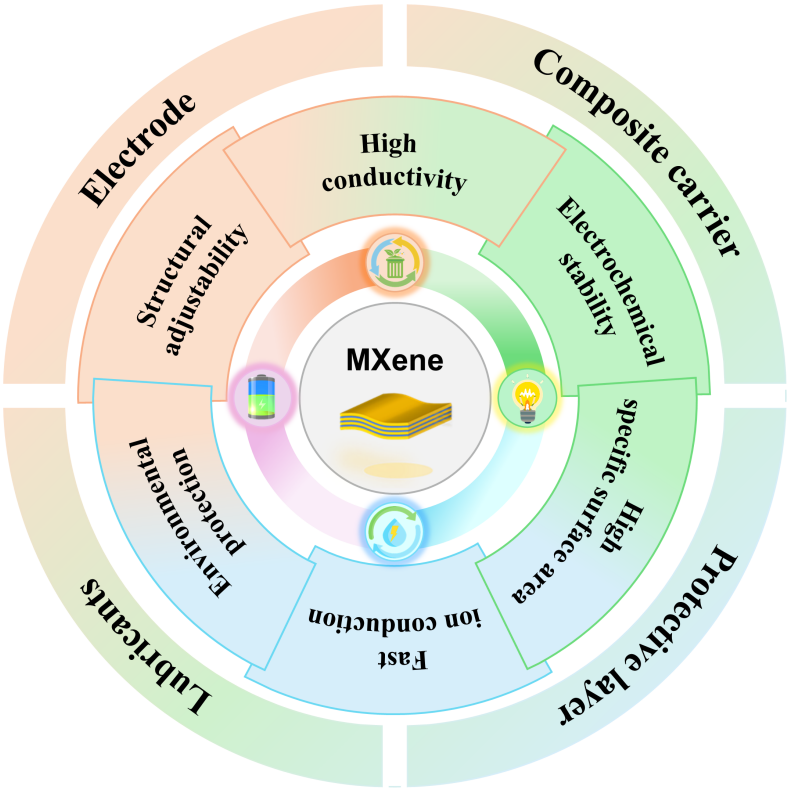

Figure 1. The characteristics and roles of MXene in the field of energy storage.

Facing the challenge of uneven distribution of lithium resources, emerging energy storage systems such as low-cost and resource-rich sodium ion batteries (SIBs) and zinc ion batteries (ZIBs) have become the key to breaking the situation. Even in the face of larger radius ions, MXene materials still show excellent adaptability and can achieve fast and stable storage [18,19]. The flexible layered structure of MXene can effectively withstand

the stress caused by the insertion and extraction of various metal ions, which provides a unique solution for the development of high-performance long-life rechargeable batteries [20,21]. Therefore, other energy storage systems such as potassium ion batteries (PIBs), magnesium ion batteries (MIBs), and aluminum ion batteries (AIBs) have also become promising research directions. In summary, the emerging 2D MXene materials show great application potential in the field of battery technology due to their high conductivity, adjustable surface chemical properties, excellent mechanical stability and rich active sites. This paper briefly reviews the research status and challenges of MXene in various energy storage systems, aiming to provide valuable reference and guidance for future research.

2. The Structure of 2D Nitride or Carbide MXene

In addition to graphene, MXene is another prominent 2D layered material that has gained attention in recent years as a popular option for rechargeable battery electrodes or electrode substrates. MXenes are metal carbides or nitrides obtained after stripping A metal from MAX phase materials, where MAX phase materials have the chemical formula $M_{n+1}AX_n$ (n = 1, 2 or 3), with M representing early transition metals such as Sc, Ti, Zr, V, Nb, Cr or Mo, and A usually representing the the third and fourth main group chemical elements, X is a C and/or N element. The resulting MXene materials can also be represented as $M_{n+1}X_nT_x$, where T represents the terminal functional groups such as -OH, -O and -F on the surface of the material. Since the discovery of $Ti_3C_2T_x$, various MXene materials have been extensively prepared and studied due to their unique properties in electronics, magnetism, and mechanics [22]. MXene has found wide application in catalysis and energy storage fields owing to its excellent electrical conductivity, hydrophilicity, stability in aqueous solutions, layered structure, abundant exposed active sites, and favorable ion transport channels. Similar to other 2D materials, MXene exhibits layer stacking, and material compounding, structural design, and element intercalation are common optimization strategies used to further enhance its properties [23]. MXene materials dominated by $Ti_3C_2T_x$ have demonstrated remarkable potential for energy storage applications, offering excellent volumetric capacity and fast electron transport [24,25]. Ongoing research continues to explore novel MXene materials and optimize their properties for a wide range of applications, making them a promising option for advanced energy storage systems and beyond. Notably, the MXene family has expanded from its initial $Ti_3C_2T_x$ form to encompass dozens of members today (Mo_2C [26,27], Nb_2C [28,29], Ti_3CN [30,31], etc.).

3. Energy Storage Mechanism and Regulation Strategy of MXene in Batteries

In traditional intercalated batteries (such as LIBs, SIBs, etc.), MXene mainly plays a role in the form of capacitive/pseudocapacitive carriers. The capacity contribution of MXene is mainly due to the surface redox reaction, while the bulk phase contribution is limited. The cathode materials of LIBs usually require high working voltage tolerance and excellent capacity, and the existing MXene materials are still insufficient in this regard. With its high specific surface area and excellent mechanical strength, MXene is more suitable as a conductive additive, electrode support or coating rather than the main active material of such batteries. For example, MXene can be used as a substrate or protective layer for the cathode of LIBs [32]. MXene has multiple advantages such as high conductivity, fast ion conduction, high specific surface area, adjustable structure and environmental protection. It can be used to construct a dual-ion energy storage device and provide significant support for lithium-ion-based dual-ion energy storage technology [33–35]. At this time, MXene is limited to an absolutely safe low-potential working environment. By redesigning the operating mechanism of the entire energy storage device, the oxidation risk is successfully avoided, and the high voltage and high energy output of the entire device is achieved [36]. It cannot be ignored that MXene (especially $Ti_3C_2T_x$) is prone to low potential oxidation in aqueous electrolyte. Therefore, the application of MXene in aqueous ZIBs is often used for interface protection or as a zinc deposition substrate to benefit from its zinc affinity and high conductivity.

In conversion batteries (such as Li-S batteries, solid-state lithium metal batteries) [37,38], MXene mainly acts as a polysulfide anchor/catalyst or lithium dendrite inhibitor. Li-S batteries have attracted much attention due to their excellent energy density and cost-effectiveness, but are often limited by severe structural damage caused by the polysulfide shuttle effect [39]. When MXene material is used as the cathode of lithium-sulfur battery, its 2D layered structure can effectively adsorb and anchor polysulfides, reduce their dissolution and diffusion in the electrolyte, thereby inhibiting the shuttle effect and improving the cycle stability of the battery [40]. The improvement of its core performance is due to the chemical adsorption of polysulfides by polar functional groups on the surface of MXene and the induction of uniform deposition of lithium ions. The excellent mechanical strength and structural stability of MXene can provide good support for the long-term cycle of lithium-sulfur batteries. However, the practical application of MXene still faces challenges, such as the reduction of active area

due to the stacking of nanosheets, the structural degradation during the cycle, and the high cost and insufficient oxidation stability in large-scale production. Optimization strategies for MXene focus on the following key areas:

(1) Interface engineering. Comparing the common effects of different functional groups (-O, -F, -OH, -S, -Cl, etc.) in battery systems. For example, -O groups typically favor metal ion adsorption and redox reactions, while -F groups may hinder ion diffusion. Introducing specific functional groups as needed or combining with other materials (graphene, conductive polymers, etc.) enhances stability and electrochemical performance [41,42]. At the atomic scale, precisely replacing surface functional groups, anchoring with single atoms/nanoparticles can effectively regulate the interfacial chemical potential and adsorption energy between MXene and active materials. This addresses the root cause of slow reaction kinetics in catalytic conversion batteries (Li-S, Na-S, etc.).

(2) Interlayer regulation. Computations determine the minimum interlayer spacing thresholds required for ions of varying radii (Li^+, Na^+, K^+, Zn^{2+}, etc.). At the nanoscale, interlayer engineering precisely controls ion transport and storage behavior within confined spaces while minimizing volume energy density losses caused by excessive interlayer spacing. Pre-intercalation of cations or organic molecules, co-embedding with solvents, and interlayer confinement catalysis serve as universal approaches [15,43,44]. These strategies not only accommodate carriers with varying radii but also alter reaction pathways (inducing solid-solid conversion of sulfur and mitigating shuttle effects), which are pivotal for achieving high volumetric energy density and efficient reversible electrochemical reactions.

(3) Structural design. Optimizing structural orientation in high-loading electrodes is an effective approach to mitigate sheet stacking and ensure rapid ion transport. Examples include heterojunction formation, vertically aligned structures, and core-shell microsphere architectures [45,46]. Vertical MXene layer orientation achieved through template design or magnetic field induction transforms current collector ion transport pathways from "indirect detours" to "direct channels", making it particularly suitable for high-rate, thick electrode designs. Additionally, MXene microsphere structures prepared via spray drying exhibit superior electrolyte wettability and structural stability.

In summary, MXene has been widely used in electrode materials, conductive additives, functional separator coatings and electrolytes of battery systems (Figure 2 and Table 1), which effectively improves battery capacity, rate performance and cycle stability [19,33–35,47–74].

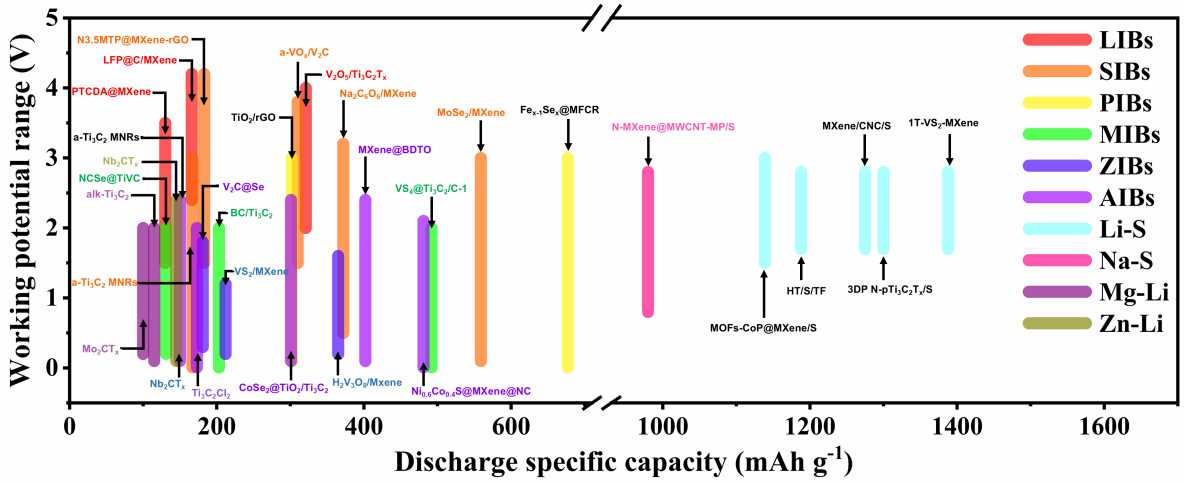

Figure 2. Application of MXene-derived electrodes in diverse rechargeable batteries.

Table 1. Common MXene-derived applications for diverse rechargeable batteries.

Battery Type	Cathode Material	Potential Range (V)	Electrolyte	Specific Capacity (mAh g^{-1})	Rate Capacity (mAh g^{-1})	Capacity Retention	Reference
LIBs	LFP@C/MXene	2.4~4.2	1 M $LiPF_6$ in EC/DEC (*v*/*v* = 1:1)	165.9 @ 0.5 C	139 @ 20 C	94.8% (156.6 mAh g^{-1} after 500 cycles @ 1 C)	[47]
	$V_2O_5/Ti_3C_2T_x$	2~4	1 M $LiPF_6$ in EC/DEC (*v*/*v* = 1:1)	321 @ 1 C	112 @ 10.5 C	91.7% (102 mAh g^{-1} after 680 cycles @ 10.5 C)	[48]
	PTCDA@MXene	1.5~3.5	1 M $LiPF_6$ in EC/DEC/EMC (*v*/*v*/*v* = 1:1:1)	129.9 @ 0.05 A g^{-1}	84.2 @ 2 A g^{-1}	62.7% (66.3 mAh g^{-1} after 1500 cycles @ 0.5 A g^{-1})	[49]
Li-S batteries	MOFs-CoP@MXene/S	1.5~3	1 M LiTFSI + 0.2 M $LiNO_3$ in DME/DOL (*v*/*v* = 1:1)	1138.8 @ 0.2 C	493 @ 6 C	70% (796.9 mAh g^{-1} after 300 cycles @ 0.2 C)	[50]
	HT/S/TF	1.7~2.8	1 M LiTFSI in DME/DOL (*v*/*v* = 1:1) with 1 wt% $LiNO_3$	1188.3 @ 0.1 C	740.1 @ 2 C	80% (592 mAh g^{-1} after 500 cycles @ 1 C)	[51]
	MXene/CNC/S	1.7~2.8	1 M LiTFSI in DME/DOL (*v*/*v* = 1:1) with 1 wt% $LiNO_3$	1275.5 @ 0.1 C	630.5 @ 4 C	64.6% (823.6 mAh g^{-1} after 100 cycles @ 0.1 C)	[52]
	1T-VS_2-MXene	1.7~2.8	1 M LiTFSI in DME/DOL (*v*/*v* = 1:1) with 1 wt% $LiNO_3$	1378.9 @ 0.1 C	517 @ 5 C	64.8% (462.9 mAh g^{-1} after 500 cycles @ 2 C)	[53]
	3DP N-p$Ti_3C_2T_x$/S	1.7~2.8	1 M LiTFSI + 0.5 M $LiNO_3$ in DME/DOL (*v*/*v* = 1:1)	1300 @ 0.05 C	988.2 @ 0.5 C	64.6% (8.47 mAh cm^{-1} after 60 cycles @ 12.02 mg cm^{-1})	[54]
SIBs	a-VO_x/V_2C	1.5~3.8	1 M $NaClO_4$ in EC/PC (*v*/*v* = 1:1) with 5 wt% FEC	310 @ 0.05 A g^{-1}	96 @ 2 A g^{-1}	56.3% (54 mAh g^{-1} after 1800 cycles @ 2 A g^{-1})	[55]
	$MoSe_2$/MXene	0.1~3	1 M $NaClO_4$ in EC/PC (*v*/*v* = 1:1) with 5 wt% FEC	559 @ 0.5 A g^{-1}	250 @ 10 A g^{-1}	85.3% (384 mAh g^{-1} after 400 cycles @ 2 A g^{-1})	[56]
	a-Ti_3C_2 MNRs	0.01~3	1 M $NaCF_3SO_3$ in DG	167 @ 0.02 A g^{-1}	85 @ 0.3 A g^{-1}	57% (53 mAh g^{-1} after 500 cycles @ 0.2 A g^{-1})	[19]
	$Na_2C_6O_6$/MXene	0.5~3.2	0.6 M $NaPF_6$ in DEGDME	372 @ 0.05 A g^{-1}	231 @ 1 A g^{-1}	74.6% (215 mAh g^{-1} after 100 cycles @ 0.2 A g^{-1})	[57]
	N3.5MTP@MXene-rGO	1.5~4.2	1 M $NaClO_4$ in EC/DEC (*v*/*v* = 1:1) with 5 wt% FEC	183 @ 0.1 A g^{-1}	122 @ 1 A g^{-1}	82% (80 mAh g^{-1} after 5000 cycles @ 2 A g^{-1})	[58]
Na-S batteries	N-MXene@MWCNT-MP/S	0.8~2.8	1 M $NaClO_4$ in EC/PC (*v*/*v* = 1:1) with 5 wt% FEC	980 @ 0.5 C	550.6 @ 5 C	88.2% (450 mAh g^{-1} after 1000 cycles @ 2 C)	[59]
PIBs	a-Ti_3C_2 MNRs	0.01~3	0.8 M KPF_6 in EC/DEC (*v*/*v* = 1:1)	141 @ 0.02 A g^{-1}	60 @ 0.3 A g^{-1}	60% (42 mAh g^{-1} after 500 cycles @ 0.2 A g^{-1})	[19]
	MXene-derived TiO_2/rGO	0.1~3	0.8 M KPF_6 in EC/DEC (*v*/*v* = 1:1)	302.8 @ 0.5 C	111.4 @ 100 C	86% (130.6 mAh g^{-1} after 1000 cycles @ 10 C)	[60]
	$Fe_{x-1}Se_x$@MFCR	0.01~3	0.8 M KPF_6 in EC/DMC (*v*/*v* = 1:1)	677.3 @ 0.1 A g^{-1}	430 @ 10 A g^{-1}	81% (348.1 mAh g^{-1} after 2000 cycles @ 10 A g^{-1})	[61]
MIBs	VS_4@Ti_3C_2/C-1	0.01~2	0.25 M APC in THF	492 @ 0.05 A g^{-1}	129 @ 1 A g^{-1}	81.7% (147 mAh g^{-1} after 900 cycles @ 0.5 A g^{-1})	[62]
	NCSe@TiVC	0.2~2	0.4 M APC in THF	131 @ 0.05 A g^{-1}	76 @ 1 A g^{-1}	84.9% (73 mAh g^{-1} after 500 cycles @ 0.5 A g^{-1})	[63]
	BC/Ti_3C_2	0.01~2	0.4 M APC in THF	203 @ 0.02 A g^{-1}	152 @ 0.1 A g^{-1}	100% (150 mAh g^{-1} after 100 cycles @ 0.05 A g^{-1})	[64]

Table 1. *Cont.*

Battery Type	Cathode Material	Potential Range (V)	Electrolyte	Specific Capacity ($mAh\ g^{-1}$)	Rate Capacity ($mAh\ g^{-1}$)	Capacity Retention	Reference
Mg^{2+}/Li^{+} batteries	Mo_2CT_x	0.2~2	0.4 M APC + 0.4 M LiCl in THF	100 @ 0.1 C	50 @ 10 C	93% (80 $mAh\ g^{-1}$ after 500 cycles @ 1 C)	[33]
	alk-Ti_3C_2	0.1~2	0.4 M APC + 1 M LiCl in THF	115.9 @ 0.1 A g^{-1}	91 @ 2 A g^{-1}	100% (96.3 $mAh\ g^{-1}$ after 1000 cycles @ 1 A g^{-1})	[34]
ZIBs	$H_2V_3O_8$/MXene	0.2~1.6	3 M $Zn(CF_3SO_3)_2$	365.3 @ 0.2 A g^{-1}	163.8 @ 2 A g^{-1}	84% (159.3 $mAh\ g^{-1}$ after 5600 cycles @ 5 A g^{-1})	[65]
	VS_2/MXene	0.2~1.2	2 M $ZnCl_2$	212 @ 0.2 A g^{-1}	108 @ 5 A g^{-1}	93.4% (101 $mAh\ g^{-1}$ after 2400 cycles @ 5 A g^{-1})	[66]
	$Ti_3C_2Cl_2$	0.3~1.8	1 M $Zn(CF_3SO_3)_2$	181 @ 0.25 A g^{-1}	81.5 @ 15 A g^{-1}	80% (68 $mAh\ g^{-1}$ after 700 cycles @ 4 A g^{-1})	[67]
Zn^{2+}/Li^{+} batteries	Nb_2CT_x	0.1~2.4	21 M LiTFSI + 1 M $Zn(OTf)_2$	145 @ 0.5 A g^{-1}	77 @ 6 A g^{-1}	95% (121 $mAh\ g^{-1}$ after 1800 cycles @ 1 A g^{-1})	[35]
AIBs	$Ni_{0.6}Co_{0.4}S$@MXene@NC	0.01~2.1	[EMIm]Cl/$AlCl_3$ (M/M = 1:1.3)	481.2 @ 0.4 A g^{-1}	294 @ 1 A g^{-1}	42.6% (125.2 $mAh\ g^{-1}$ after 300 cycles @ 1 A g^{-1})	[68]
	V_2C@Se	0.1~2.4	[EMIm]Cl/$AlCl_3$ (M/M = 1:1.3)	402.5 @ 1 A g^{-1}	120 @ 3 A g^{-1}	30% (119.8 $mAh\ g^{-1}$ after 1000 cycles @ 1 A g^{-1})	[69]
	MXene@BDTO	0.1~2.4	[EMIm]Cl/$AlCl_3$ (M/M = 1:1.3)	301.4 @ 0.5 A g^{-1}	150.4 @ 3 A g^{-1}	70% (140 $mAh\ g^{-1}$ after 500 cycles @ 0.5 A g^{-1})	[70]
	Nb_2CT_x	0.1~2.4	[EMIm]Cl/$AlCl_3$ (M/M = 1:1.3)	150 @ 0.05 A g^{-1}	50 @ 0.5 A g^{-1}	50% (76 $mAh\ g^{-1}$ after 300 cycles @ 0.2 A g^{-1})	[71]
	$CoSe_2$@TiO_2/Ti_3C_2	0.01~2	[EMIm]Cl/$AlCl_3$ (M/M = 1:1.3)	173 @ 0.2 A g^{-1}	102 @ 3.2 A g^{-1}	100% (173 $mAh\ g^{-1}$ after 100 cycles @ 0.2 A g^{-1})	[72]

4. The Synthesis Method of MXene and Its Behavior in Batteries

It is worth noting that the synthesis strategy is directly related to the actual performance of MXene. MXenes prepared by different etching methods have significant differences in interlayer spacing, defect density, functional group type and distribution, and lamellar size, which directly affect their behavior in batteries. Fluorine-containing etching methods (such as direct HF etching, MILD method based on HCl and fluoride salts, molten salt etching) are the most mature and widely used strategies for synthesizing MXene [22]. Its core advantage is that it can efficiently and selectively remove the A layer in the MAX phase to obtain a 2D layered structure. Among them, the MILD method can prepare high-quality MXene with larger lamellar size and fewer defects by virtue of its relatively mild reaction conditions and cation intercalation effect. Its excellent electrical conductivity and electrochemical performance make it show great potential in the fields of energy storage and electromagnetic shielding. The molten salt method breaks through the limitation of HF etching on the MAX phase of the precursor, and can synthesize a new type of MXene with A layer of Si, Ga and other elements, and endow it with unconventional surface functional groups such as-Cl and-Br, which greatly expands the material family and performance exploration space of MXene. However, the shortcomings of such methods are also obvious: direct use of HF or in-situ generation of HF involves highly toxic fluorine-containing reagents, and there are safety risks and environmental protection pressures; although the molten salt method has good environmental adaptability, the current yield and product conductivity are far less than the MILD method. In addition, the surface of MXene obtained by fluorine-containing etching usually has mixed functional groups such as-F, -O, and-OH. This complex surface chemistry sometimes facilitates specific applications such as catalysis, but it increases uncertainty for raw materials that require precise regulation of interface properties.

In order to avoid the safety risks and uncontrollable surface chemistry of highly toxic and highly corrosive HF etching, Huang's team pioneered a novel MXene preparation process based on the molten salt method, enriching the diversity of MXene species while avoiding the harmful effects of hydrofluoric acid [75]. A judgment basis for judging whether the molten salt can be used for stripping is integrated based on the redox potential of the cation. The MAX phase (Ti_3AlC_2) in molten Lewis acid would undergo a displacement reaction similar to that in hydrofluoric acid, resulting in a $M_{n+1}ZnX_n$ phase and a novel MXene with Cl surface. Under the guidance of this judgment, a variety of MXene products ($CdCl_2$, $FeCl_2$, $CoCl_2$, $CuCl_2$, AgCl, $NiCl_2$) were synthesized through the molten salt etching process of MAX phases (Ti_2AlC, Ti_3AlC_2, Ti_3AlCN, Nb_2AlC, Ta_2AlC, Ti_2ZnC and Ti_3ZnC_2) [76]. Ti_3C_2 obtained by exfoliating Ti_3SiC_2 with $CuCl_2$ molten salt achieved an exceptional storage capacity as high as 205 mAh g^{-1} while retaining wide operating voltage window of 0.2~3 V. To improve the low surface area of MXenes and the inhomogeneous edge termination produced by dangerous high-frequency etching. Chen et al. first synthesized chloro-terminated MXene with tunable in-plane porosity using a eutectic hybrid etching strategy (Figure 3a–g) [77]. The pore structure of MXene was tightly protected by controlling the temperature and composition of the NaCl/$ZnCl_2$ salt mixture. The final porous MXene $Ti_3C_2Cl_2$ has high mesoporous ratio and high specific surface area, and its Li^+ diffusion barrier is only 0.2 eV.

Zhi et al. synthesized halogenated MXenes with different halogen end functional groups (-Cl, -Br, -I, -BrI, and -ClBrI) based on a molten salt etching strategy, revealing the significance of different surface-active terminals for tuning the material properties [67]. The electrochemical activity of -Br and-I elements endows MXene with excellent electrochemical performance. $Ti_3C_2Br_2$ and $Ti_3C_2I_2$ have the highest reversible discharge capacity of 135 mAh g^{-1} when used as the positive electrode of aqueous ZIBs. And the capacity of binary Ti_3C_2(BrI) and ternary Ti_3C_2(ClBrI) with double discharge plateau characteristics were as high as 117.2 and 106.7 mAh g^{-1}, respectively, which is much better than that of conventional $Ti_3C_2Cl_2$ (only 46.5 mAh g^{-1}) without plateau behavior (Figure 3h,i). Furthermore, the complete electron transfer and abundant valence supply of rechargeable zinc-iodine conversion batteries in the energy storage process are fully revealed, showing the unique characteristics and potential of halogenated MXene in energy storage applications [78]. Electronegative F^- and Cl^- ions help to stabilise I^+ during charging, and tailored electrolytes based on F^- and Cl^- ions have a positive effect on the activation of reversible I^0/I^+ redox behavior at potentials of 0.99 V. $Ti_3C_2I_2$ exhibited only a single I^0/I^+ redox reaction at ~0.54 V, which results in a low voltage plateau at 1.30 V for ZIBs (Figure 3j–m). Whereas in the optimized Cl-rich $ZnCl_2$ + KCl aqueous electrolyte, the I-terminal halogenated $Ti_3C_2I_2$ MXene cathode exhibited two well-defined discharge plateaus at 1.65 V and 1.30 V (corresponding to 108% capacity improvement and 231% energy density improvement). Yang's team has developed an innovative in-situ induced etching strategy to fabricate a three-dimensional interconnected porous MXene/Carbon Quantum Dots (MXene/CDs) electrode via a simple solution intermixing-assisted vacuum filtration treatment [79]. The CDs are uniformly distributed in the pre-intercalated layers between the MXene layers, effectively addressing the challenge of easy stacking of MXene nanosheets. The uniform in-plane macropores formed by the partial decomposition of the CDs during annealing reduce the tortuosity of ion migration paths in the vertical direction and the migration potential barrier.

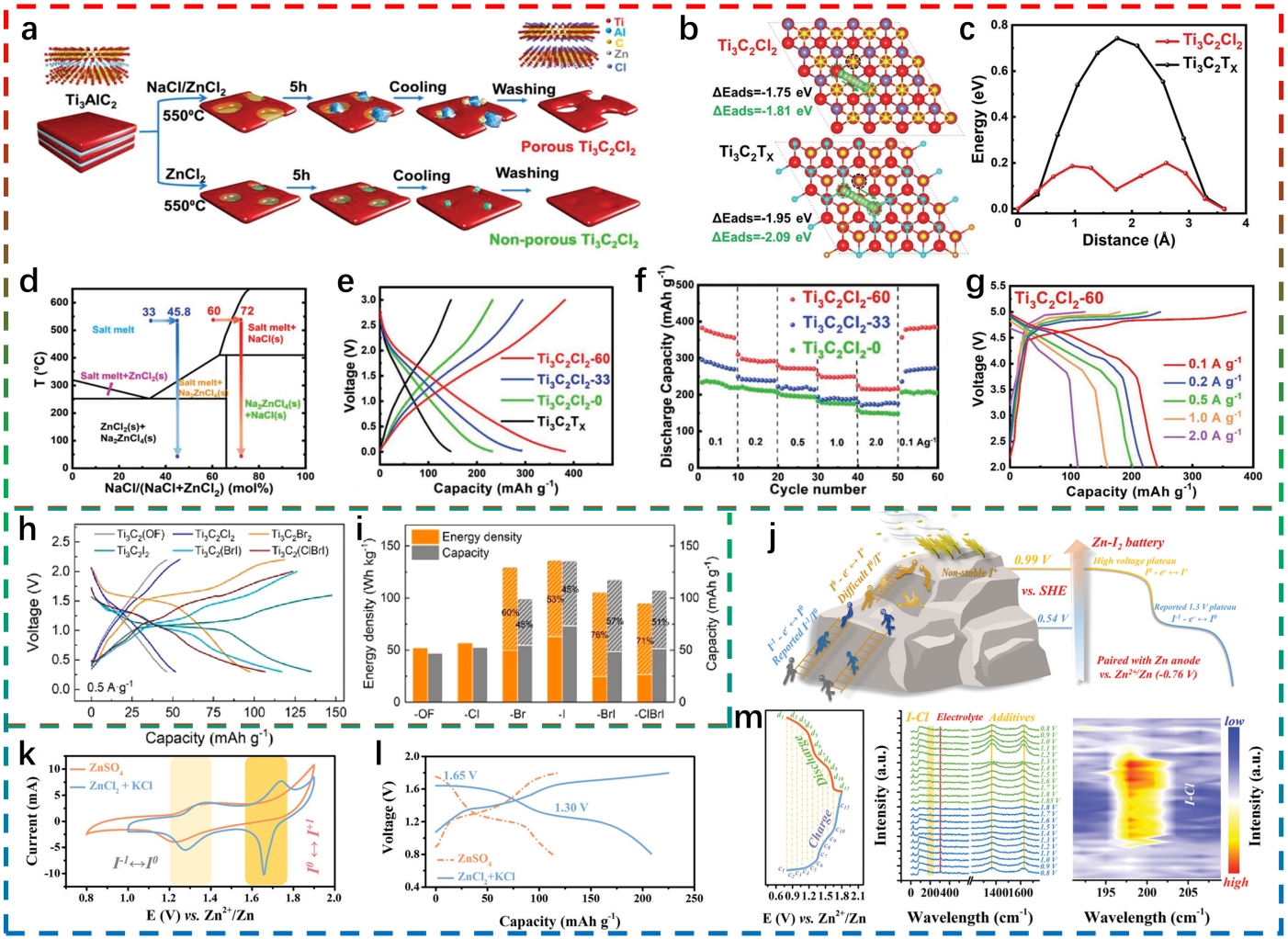

Figure 3. (**a**) Schematic illustration of in-plane porous $Ti_3C_2Cl_2$ synthesized by MAX and salt mixture; (**b**) Adsorption energy of energetically favorable sites, and (**c**) diffusion barrier profiles of Li ion hopping migration on the selected terminations of $Ti_3C_2Cl_2$ and $Ti_3C_2O_{0.1}F_{1.4}(OH)_{0.5}$ surfaces; (**d**) Phase diagram of NaCl/$ZnCl_2$ (blue and red lines represent the reaction process of $Ti_3C_2Cl_2$-33 and $Ti_3C_2Cl_2$-60); (**e**) GCD curves at 0.1 A g^{-1} and (**f**) rate capability test of $Ti_3C_2Cl_2$-0, $Ti_3C_2Cl_2$-33, $Ti_3C_2Cl_2$-60, and $Ti_3C_2T_X$; (**g**) GCD curves of $Ti_3C_2Cl_2$-60.Reproduced with permission [77]. Copyright 2022, Wiley-VCH. (**h**) Typical GCD curves of Ti_3C_2 MXene with different terminals at 0.5 A g^{-1}; (**i**) Energy density and capacity of Ti_3C_2 MXene with different terminals. Reproduced with permission [67]. Copyright 2022, American Chemical Society. (**j**) Illustration of the reactions of I_2//Zn battery; (**k**) CV curves at 10 mV s^{-1} and (**l**) GCD curves at 0.5 A g^{-1} of $Ti_3C_2I_2$//Zn battery based on optimized $ZnCl_2$ + KCl electrolyte and conventional $ZnSO_4$ electrolyte; (**m**) GCD curve with marked voltage points for in situ Raman spectra of the $Ti_3C_2I_2$ cathodes and Refined Raman map. Reproduced with permission [78]. Copyright 2021, The Royal Society of Chemistry.

HF produces a large number of -F surface end groups during MXene etching, which leads to high hydrophobicity, poor zinc affinity and delayed ion diffusion kinetics. In order to overcome these difficulties, Liu et al. have prepared a novel K^+ pillar-supported hydroxyl-terminated V_2CT_x-rich MXene material (alk-V_2CT_x) by a facile and controllable one-step alkalization method [80]. The hydroxyl-rich group weakens the electrostatic interaction between the host and the zinc ion and accelerates the ion diffusion, the pre-insertion of K^+ as a support effectively stabilizes the layered structure of the material and expands the interlayer spacing. The alk-V_2CT_x exhibits highly reversible Li^+/Zn^{2+} co-insertion/co-deinsertion behaviour. And the alk-V_2CT_x exhibits excellent multiplicative performance (reversible capacities of 498.2 and 195.1 mAh g^{-1} at 0.1 and 30 A g^{-1}, respectively) and excellent cycle life (96.2% capacity retention after 20000 cycles) in 15 M LiTFSI + 1 M $Zn(CF_3SO_3)_2$. In situ characterization and calculations have revealed that the embedding/de-embedding behavior of Zn^{2+} dominates the capacity in the high-voltage region (1.6~0.5 V), while the embedding/de-embedding chemistry of Li^+ activates the capacity in the low-voltage region (0.5~0.2 V). Feng et al. have introduced a surface grafting method using multifunctional azobenzene sulfonic acid to convert V_2C MXene into a high-kinetic K^+ intercalation electrode [21]. The grafted azobenzenesulfonic acid not only provides an additional storage center and a fast hopping site for K^+, but also plays a supporting role between the V_2C layers to reduce the structural distortion during the K^+ intercalation/deintercalation process, which opens up new possibilities for the development of bionic energy storage devices that can simultaneously achieve high energy density and output power density.

5. Study on the Performance of MXene-Based Materials in Different Battery Systems

Thanks to its excellent comprehensive performance, MXene material has emerged as a promising electrode material for various metal ion batteries, particularly when used in composite electrodes. Fan's team demonstrated a pre-lithium intercalated V_2C MXene nanostructure synthesized using a self-generated strategy using Li^+ storage [81]. Li^+ pre-intercalation can effectively alleviate the Li^+ loss caused by the formation of the solid-electrolyte interface in the early stage of the battery by providing an alternative lithium source. At the same time, the intercalation of Li^+ significantly expands the interlayer spacing of MXenes, providing rich active sites and fast channels for ion transport. V_2C not only provided a high reversible capacity of 547.5 mAh g^{-1} when used as an anode for LIBs, but also had a reversible capacity of 230.3 mAh g^{-1} as a cathode for Mg/Li hybrid battery due to the cross-linking intercalation mechanism. Ex-situ XRD measurements reveal that the (002) peak of V_2C-10 gradually shifts from 8.03° to 7.62° during discharge to 0.01 V, reversibly recovering to 8.02° after charging to 2.0 V. This corresponds to the expansion and contraction of the interlayer spacing in V_2C-10 during Mg^{2+}/Li^+ ion insertion and extraction. Magnesium migration dynamics in oxygen-functionalized V_2C MXene (labeled V_2CO_2) were calculated using density functional theory (DFT). As the number of layers decreases, the Mg^{2+} migration energy barrier in monolayer V_2CO_2 can be reduced to 0.59 eV. The increased interlayer spacing resulting from Li^+ ion pre-intercalation provides additional ion diffusion pathways, contributing to the fast reaction kinetics and high Mg^{2+} ion storage capacity of V_2CO_2 MXene.

MOFs-derived composites have unique polyhedral structures and defects, which have great potential in improving adsorption capacity and redox catalytic activity. MXene has excellent graphene-like structure and good structural stability, and exhibits excellent capacitance characteristics when it can form a three-dimensional network with high conductivity with active materials. Zong et al. self-assembled metal-organic framework-derived CoP in Ti_3C_2 MXene to optimize ion diffusion kinetics and capacity decay of the electrode [50]. As the cathode of lithium-sulfur battery, MOFs-CoP@MXene has stable sulfur electrochemical performance and can effectively inhibit the shuttle effect. The 3D composite MOFs-CoP@MXene network showed impressive performance as both anode and cathode, delivering excellent long-term cycling stability and enhanced ion diffusion kinetics. Zhong et al. reported a scalable drop casting method to obtain large-area independent MXene $Ti_3C_2T_x$ films (Figure 4a–g) [51]. This film can significantly improve the adhesion of the sulfur layer under continuous bending when used in lithium-sulfur batteries. The unique sandwiched cathode composed of a large-scale $Ti_3C_2T_x$ film and TiO_2/H-$Ti_3C_2T_x$ provides a continuous electron transport path as well as adsorption sites and flexibility for LIBs. The top and bottom layers of MXene can not only be used as current collectors to improve the conductivity of the electrode, but also serve as an effective reservoir for dissolving lithium polysulfides to inhibit their diffusion and buffer volume changes. No voltage change was observed in the flexible lithium-sulfur battery based on this structure after 3500 bending cycles. Zhang et al. conducted an electrochemical oxidation process to transform the outer surface of V_2CT_x into an amorphous nano-VO_x layer encapsulated in situ on the V_2CT_x substrate (a-VO_x/V_2C) [55]. The a-VO_x layer ensures reversible insertion/detachment and rapid diffusion of Na^+ by providing sufficient vacancies and open channels in the amorphous framework. while the V_2C layer serves as a conductive and robust backbone to accelerate efficient ion/electron transport while safeguarding the structural integrity (Figure 4h,l). In-situ Raman

spectroscopy, in-situ transmission electron microscopy, and in-situ synchrotron X-ray absorption spectroscopy clearly reveal the enhanced reversibility and structural advantages of the a-VO_x/V_2C nanohybrid material: reversible V-O vibrations and oscillation between V^{4+} and V^{5+} valence states are achieved within the disordered framework. Given the isotropic nature of the a-VO_x framework, Na^+ can diffuse along random directions. DFT results further reveal that a-VO_x forms zigzag channels, with interconnected Na^+ diffusion pathways exhibiting low diffusion barriers and significantly advantageous ionic intercalation volume changes.

Similarly, Xu et al. achieved the in-situ assembly of $MoSe_2$/MXene heterojunctions to improve the sluggish electrochemical kinetics of large-sized Na^+ through a simple hydrothermal-thermal annealing two-step strategy [56]. The van der Waals force interaction between $MoSe_2$ and MXene effectively suppressed the volume change during the insertion/withdrawal of sodium ions. Meanwhile, DFT calculations demonstrated that the unique reticular heterostructure based on MXene has high electrical and ionic conductivity (low diffusion impedance between Na^+/MXene of ~0.066 eV), which is very favourable for sodium ion transport. The final electrode achieves excellent rate performance and long cycling capability, and the $MoSe_2$/MXene heterojunction shows a high reversible capacity 250 mAh g^{-1} and a Coulombic efficiency of close to 100% even at a high current of 10 A g^{-1}. Liu et al. demonstrated the in-situ growth of highly stable non-oriented $H_2V_3O_8$ nanowires directly on MXene nanosheets as a promising cathode for aqueous ZIBs [65]. 2D Mxene sheets not only guide the growth of $H_2V_3O_8$ nanowires, but also bond $H_2V_3O_8$ nanowires together to form a three-dimensional aligned structure with high conductivity. The $H_2V_3O_8$/MXene composite structure shows enhanced conductivity and higher charge transfer efficiency, and the reversible co-doping electrochemical reaction mechanism of Zn^{2+} with water further improves the rate performance of the cell. Particularly the solid-state ZIBs based on polyacrylamide/cellulose nanofiber hydrogel electrolyte exhibited a high discharge capacity of 317.4 mAh g^{-1} and wide voltage operating range of −18~40 °C. These studies showcase the significant potential of surface-modified MXene-based composite cathodes for various types of batteries. The ability to enhance electrochemical performance, rate ability, and stability through surface regulation and heterojunction assembly highlights the versatility and promise of MXene-based materials in advancing energy storage technologies.

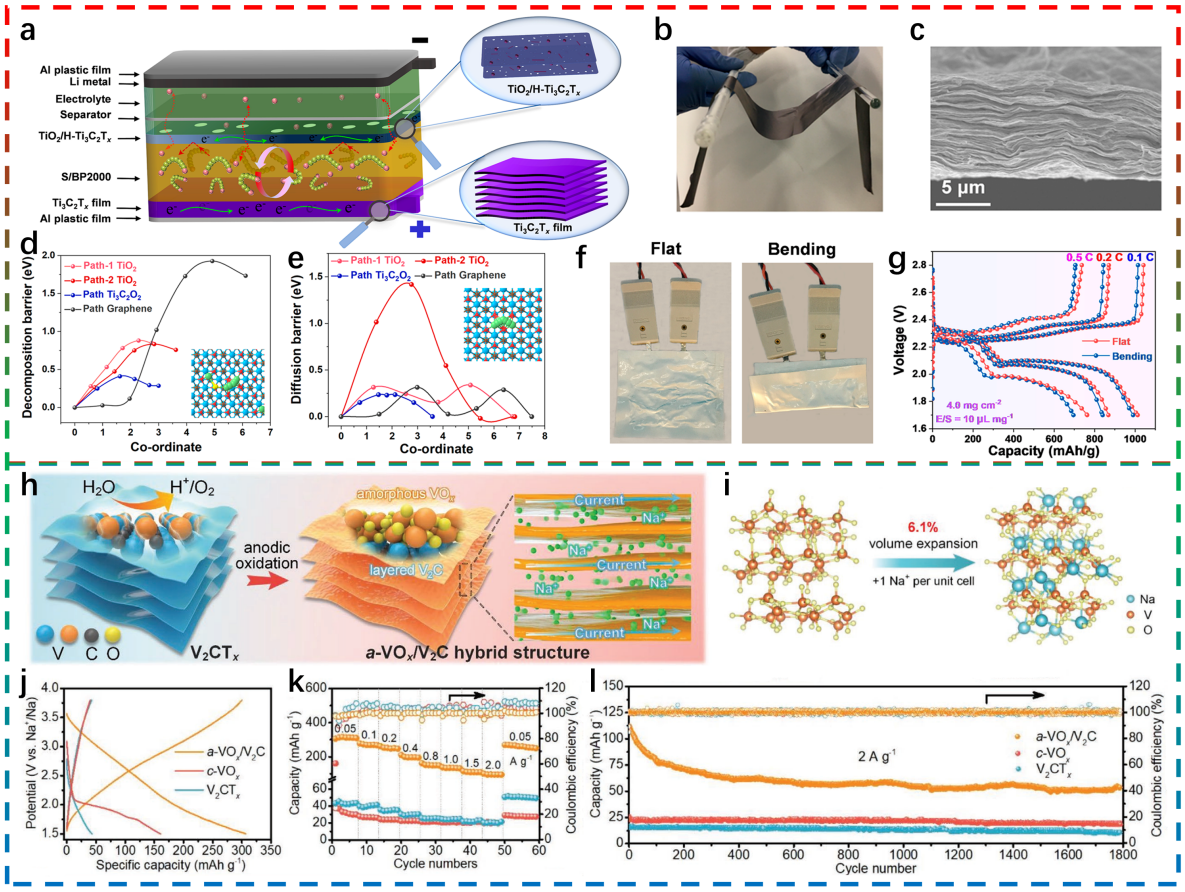

Figure 4. (**a**) Schematic of flexible Li-S battery using the $Ti_3C_2T_x$ film as the current collector and TiO_2/H-$Ti_3C_2T_x$ as the coating layer; (**b**) Optical image of a large-area $Ti_3C_2T_x$ film; (**c**) Cross-sectional SEM image of the $Ti_3C_2T_x$ film. Barriers to (**d**) Li_2S decomposition and (**e**) Li ions diffusion on TiO_2, $Ti_3C_2O_2$, and graphene; (**f**) Optical photographs of flexible Li-S pouch cell at flat and bent states; (**g**) Rate of a flexible Li-S battery in flat and bent

conditions. Reproduced with permission [51]. Copyright 2022, American Chemical Society. (**h**) Schematic illustration showing the synthesis and structure of a-VO_x/V_2C nanohybrid; (**i**) Structural volume change in a-VO_x during the insertion of 1 Na^+ per unit cell; (**j**) The first cycle charge-discharge profiles of pristine V_2CT_x, c-VO_x, and a-VO_x/V_2C electrodes at 50 mA g^{-1}; (**k**) Rate capability of the samples from 50 mA g^{-1} to 2000 mA g^{-1}; (**l**) Cycling performances of the three samples at 2000 mA g^{-1}. Reproduced with permission [55]. Copyright 2021, Wiley-VCH.

The optimization of MXene through structural manipulation [19], targeted heteroatom coordination [82], and terminal functional group manipulation [67] has been a key focus of research. Properly adjusting the interlayer spacing of MXene nanosheets, such as through alkalization, has proven to be an effective means of enhancing performance. Wu's group reported the energy storage behavior of alkali-treated Ti_3C_2 MXene nanoribbons (a-Ti_3C_2 MNRs) [19]. This unique structure synergistically combines a three-dimensional open porous network consisting of nanoribbons with extended layer spacing to achieve fast electron transport and rapid ion diffusion. The ionic reaction kinetics and structural stability of the electrodes have been significantly enhanced thanks to the widened a-Ti_3C_2 layer spacing, narrowed nanoribbon widths, and three-dimensional interconnected porous frameworks. The a-Ti_3C_2 MNRs showed excellent storage performance for both SIBs and PIBs (168 and 136 mAh g^{-1} at 20 mA g^{-1}, respectively). Zhao et al. adopted a self-sacrificial template strategy to process 2D MXene sheets into hollow spheres with 3D structures [83]. The MXene hollow spheres have good stability and dispersibility in water and ethanol. The three-dimensional macroporous MXene film synthesized based on MXene hollow spheres has the advantages of flexibility and high conductivity due to the good contact between the spheres and the metal conductivity of MXene. The prepared 3D free-binder $Ti_3C_2T_x$, V_2CT_x, and Mo_2CT_x film electrodes exhibited maximum reversible capacity of 330, 340, and 370 mAh g^{-1} for Na-ion storage, respectively.

Zhu et al. synthesized 3D interwoven Ti_3C_2 MXene networks (BC/Ti_3C_2) and a 2D multilayer hybrid material (VS_4@Ti_3C_2/C), both of which demonstrated remarkable discharge capacity of 171 mAh g^{-1} as cathodes for rechargeable MIBs [64]. The tuned BC/Ti_3C_2 has a larger interlayer spacing (d = 1.8 nm) than the pristine pure Ti_3C_2 (d = 1.4 nm). Later, Zhu et al. further synthesized a 2D multilayer hybrid material (VS_4@Ti_3C_2/C) with a hierarchical nano-microstructure by anchoring VS_4 nanosheets on a carbon-coated Ti_3C_2 MXene matrix [62]. The unique hierarchical multilayer structure of the VS_4@Ti_3C_2/C facilitated rapid electrolyte penetration and reduced charge transport resistance. Non-aqueous MIBs based on VS_4@Ti_3C_2/C cathode and magnesium foil anode acquired an impressive capacitance and excellent rate performance. The corresponding chemical states of VS_4 can be analyzed in detail based on in-situ XRD and XPS spectra during charging and discharging. During the first discharge cycle, $PY14^+$ ions predominantly drive the expansion of adjacent chains in VS_4. Consequently, when discharged to 0 V, the two main peaks of VS_4 gradually diminish and eventually disappear, attributed to the insertion of $PY14^+$ and $MgCl^+$ ions. The absence of the VS_4 main peak during charging indicates that $PY14^+$ ions remain retained within the VS_4 lattice. Despite the extremely low Ti_3C_2 content in the entire composite material, changes in the XRD and XPS spectra confirm that the magnesium/demagnesium mechanism of vanadium in VS_4@Ti_3C_2/C-1 follows an intercalation/deintercalation mechanism. Modulating ion-solvent interactions offers a powerful approach to regulate desolvation processes, thereby optimizing the capacity and kinetics of electrochemical charge storage. This complex influence remains to be explored in 2D MXenes. The effect of acetonitrile (ACN) as a cosolvent on the Na^+ solvation structure and charge storage mechanism of $Ti_3C_2T_x$ MXenes is further investigated [84]. The addition of ACN enables $Ti_3C_2T_x$ to undergo a novel intercalation process at relatively positive potentials. Continuous variation in ACN content causes the charge storage mechanism of this additional process to shift from a non-Faradaic process to a redox-active process (Figure 5a–e). At lower ACN concentrations, strongly solvated Na^+ ions rapidly intercalate via a predominant non-Faradaic process, achieving superior rate retention (72% at 1 V s^{-1}). DFT results indicate that at low ACN content, ACN molecules primarily interact with water via dipole-dipole interactions, while Na^+ ions are predominantly solvated by water molecules. Higher ACN content (>50%) promotes ion desolvation, where increased ACN molecules and ClO_4^+ coordinate with Na^+ ions, weakening interactions between Na^+ and water. This ultimately yields distinct redox activity but reduced rate performance. These findings demonstrate a clear correlation between solvation structures and charge storage mechanisms in 2D MXenes, providing rational guidance for designing co-solvent strategies.

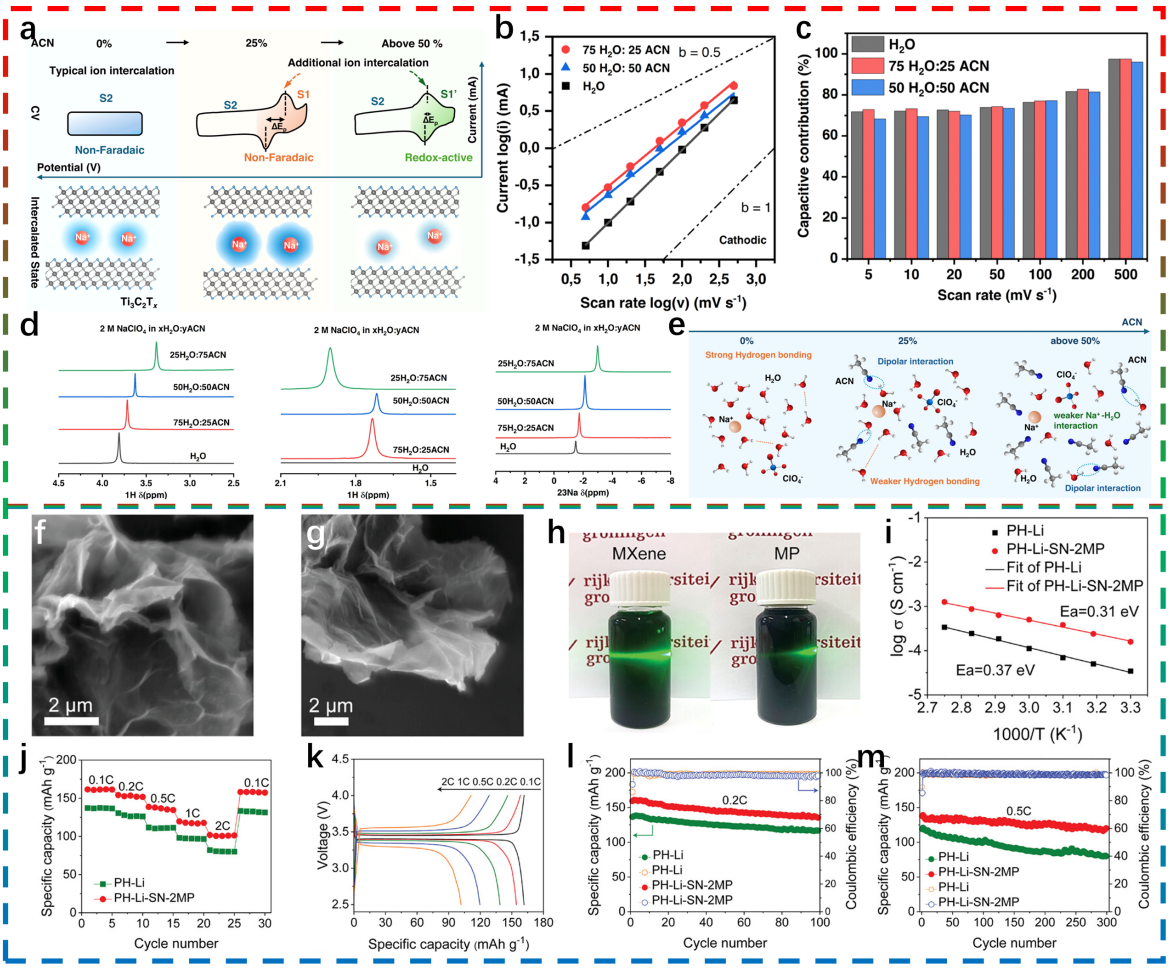

Figure 5. (**a**) Cyclic voltammograms and corresponding charge storage mechanisms of $Ti_3C_2T_x$ MXene in 2 M $NaClO_4$ with varying ACN content; (**b**) Linear fitting of logarithm of cathodic peak currents log(i) versus the logarithm of scan rates log(v) for $Ti_3C_2T_x$; (**c**) Surface-contributed capacitance contribution at different scan rates; (**d**) ^1H NMR spectra of water, ACN and ClO_4^-; (**e**) Schematic illustration showing evolution of Na^+ ion solvation structure with increased ACN ratio. Reproduced with permission [84]. Copyright 2025, Elsevier. SEM image of (**f**) MXene and (**g**) MP; (**h**) Tyndall effect of MXene and MP dispersed in DMF; (**i**) Arrhenius plots of ionic conductivities for PH-Li and PH-Li-SN-2MP SPEs; (**j**) Rate capabilities of Li/PH-Li/LFP and Li/PH-Li-SN-2MP/LFP cells; (**k**) Charge/discharge curves of the Li/PH-Li-SN-2MP/LFP cells at various rates; (**l**) Cycling performance of Li/PH-Li/LFP and Li/PH-Li-SN-2MP/LFP cells at 0.2 C; (**m**) Cycling performance of Li/PH-Li/LFP and Li/PH-Li-SN-2MP/LFP cells at 0.5 C. Reproduced with permission [85]. Copyright 2025, Wiley-VCH.

6. The Application of MXene in Solid-State Batteries

Solid-state batteries are considered a key direction for next-generation batteries due to their high safety and potential for high energy density. However, they currently face challenges such as high interfacial resistance, poor mechanical properties, and low ion transport efficiency. MXene, with its exceptional conductivity, tunable surface chemistry, and excellent mechanical flexibility, demonstrates significant application potential in multiple aspects of solid-state batteries, including electrolytes, electrode materials, interfacial layers, and current collectors. Currently, MXene is primarily applied in LIBs and lithium-sulfur batteries within solid-state battery systems.

Masashi Okubo et al. combined in-situ scanning transmission electron microscopy (STEM) with electron energy loss spectroscopy (EELS) to observe the lithium storage behavior in multi-layer $Ti_3C_2T_x$/$70Li_2S{\cdot}30P_2S_5$ solid electrolyte composite system at room temperature and high temperature in real time [86]. Dynamic imaging of lithium distribution within $Ti_3C_2T_x$ and at the $Ti_3C_2T_x$/solid electrolyte interface revealed that charge storage follows a hybrid mechanism involving conversion and intercalation reactions. The energy storage process involves three concurrent reactions: (i) Reversible interlayer lithium intercalation in MXene accompanied by titanium redox reactions; (ii) Partially reversible growth and decomposition of a nanoscale Li_2O film on the surface; (iii) Reductive decomposition of sulfide electrolyte at the electrode interface. At 80 °C, the inert $Ti_3C_2T_x$ layers at room temperature become activated. O-terminated sheets initially exhibit higher titanium oxidation states and faster

lithium adsorption rates, while divalent O-terminated sheets favor lithium accommodation and redox utilization while simultaneously promoting Li_2O formation to increase irreversible capacity.

Giuseppe's team developed a novel solid-state polymer electrolyte by covalently grafting methoxy polyethylene glycol (mPEG) onto MXene surfaces to enhance MXene dispersion and compatibility within a polyvinylidene fluoride-hexafluoropropylene matrix [85]. The compatibility between modified MXene and PH was significantly enhanced. By uniformly dispersing 2D MXene nanosheets within a plasticized polyvinylidene fluoride-hexafluoropropylene matrix, the dissociation of lithium salts in the solid polymer electrolyte was markedly improved through the synergistic effect of the plasticizer succinyl succinic acid (Figure 5f–m). This solid polymer electrolyte exhibits ionic conductivity and Li^+ mobility of 1.49×10^{-4} S cm^{-1} and 0.59, respectively, at 30 °C, and demonstrates stable reversible lithium plating behavior exceeding 2100 h in Li/Li symmetric cells.

To address the low room-temperature ionic conductivity of poly(ethylene oxide) (PEO) solid polymer electrolytes and the low mechanical strength of succinonitrile (SN) plasticizers, Hu's team incorporated $Ti_3C_2T_x$ with surface-enriched competitive functional groups into the PEO/SN-based solid electrolyte system. Benefiting from hydrogen bonding interactions between SN and $Ti_3C_2T_x$, direct contact between SN molecules and the lithium anode, along with associated corrosion issues, was significantly mitigated. The competitive coordination-induced effect (CCIE) triggered by competitive functional groups in $Ti_3C_2T_x$ weakened the Li^+ coordination environment, lowered the Li^+ migration barrier, and ultimately enabled efficient Li^+ transport. The PEO/SN/0.8$Ti_3C_2T_x$ electrolyte synthesized by adjusting the $Ti_3C_2T_x$ ratio exhibits high ionic conductivity (2.17×10^{-3} S cm^{-1}) at 35 °C. A lithium symmetric cell assembled with the PEO/SN/0.8 $Ti_3C_2T_x$ electrolyte demonstrated outstanding cycling stability exceeding 5000 h at 0.2 mA cm^{-2}/0.2 mAh cm^{-2} and 28 °C, maintaining a cycle life of 4500 h even at 0.05 mA cm^{-2}/0.05 mAh cm^{-2} and −5 °C. This approach provides a simple and effective strategy for preparing PEO/SN-based solid-state electrolytes with high ionic conductivity and constructing stable electrode/electrolyte interfaces.

MXene has emerged as a versatile platform in solid-state battery technology due to its high conductivity and unique 2D layered structure. It primarily functions as an additive to enhance the ionic conductivity and mechanical strength of solid-state electrolytes, serves as an electrode framework to buffer volume expansion, and acts as an interfacial layer to reduce impedance while effectively suppressing the growth of anode metal dendrites, thereby improving overall battery stability.

7. The Role and Optimization Mechanism of MXene in Different Components of the Battery

The inherent metal-level conductivity of MXene lays the foundation for its application as an efficient conductive pathway in all battery systems. Its layered structure provides a short-range pathway for ion transport and acts as a buffer matrix to adapt to the significant volume change of the electrode during charging and discharging. At present, MXene has been applied to many energy storage systems such as LIBs, SIBs, ZIBs, Li-S batteries and so on. In summary, MXene materials play a multi-dimensional regulatory role in rechargeable batteries.

In the cathode field, MXene is mainly used as a conductive skeleton or functional composite component to overcome the problems of poor conductivity, easy dissolution and structural collapse of traditional cathode materials. By integrating the active material into the MXene framework, an efficient ion / electron transport channel can be constructed, which can significantly improve the intrinsic conductivity of the active material and accelerate the ion diffusion kinetics. MXene with excellent mechanical strength and flexibility can also be used as a buffer layer to inhibit the volume expansion and irreversible phase transition of the active material during the long cycle process, thereby maintaining the integrity of the electrode structure and achieving ultra-long cycle life. In the field of relatively mature LIBs, MXene can be used to solve the self-stacking problem in anode materials such as fluorinated graphite. When combined with other materials, MXene can form a heterostructure, increase the interlayer spacing and introduce a built-in electric field, which accelerates the transport of electrons/ions, while retaining its metal-level conductivity and 2D layered structure, thereby improving lithium storage capacity and rate performance. For larger radius ions, MXene provides a fast ion adsorption/desorption pathway for the entire electrode material by capacitively enhancing or expanding the interlayer spacing, achieving a transition to a capacitive adsorption mechanism supported by high conductivity, effectively compensating for the ion kinetic diffusion rate. In lithium-sulfur batteries, MXene is both a host of sulfur and an electrocatalyst. The polar multi-functional groups on the surface of MXene can chemically adsorb polysulfides with high affinity, accelerate their redox transformation, prevent them from dissolving into electrolytes, and significantly improve the utilization rate and cycle life of sulfur cathodes. At the same time, the catalytic active sites of MXene can reduce the reaction energy barrier, accelerate the solid-liquid-solid multiphase transformation, and inhibit the shuttle effect of polysulfides.

In the anode field, MXene materials provide an effective solution for solving dendrite growth and optimizing interface stability through interface engineering and structural design. The rich functional groups on the surface of

MXene have affinity for some metals, which can be used as uniform nucleation sites to reduce the nucleation overpotential. The electric field at the anode interface can be redistributed by constructing a highly conductive MXene artificial interface layer. The artificial interface layer can not only act as a physical barrier to inhibit side reactions, but also guide the uniform nucleation and deposition of metal cations, and ultimately achieve the goal of reducing side reactions and fundamentally inhibiting dendrite growth. Some MXenes modified with functional groups can also induce the directional preferential growth of metal cations along the crystal plane. This dense and flat deposition morphology can effectively prevent dendrites from piercing the separator.

In addition to electrode materials, MXene is also used to optimize electrolytes and separators to achieve a more uniform ion flux and a more stable interface. For example, in aqueous ZIBs, MXene or its derivatives can spontaneously assemble into a protective layer on the surface of the zinc anode after being added to the electrolyte as a functional additive, which plays a similar role as the artificial interface layer. In addition, the coating of MXene layer on the separator can also optimize ion transport and interface environment. This functionalized separator helps to homogenize the metal cation flux and may capture harmful by-products through its surface chemical properties, thereby further improving the coulombic efficiency and cycle life of the battery.

In the solid electrolyte, the MXene material first plays a key optimization role in the electrolyte as a functional filler. Its abundant surface functional groups can bind to lithium salt anions (such as $TFSI^-$) through interaction, effectively promoting the dissociation of lithium salts and greatly increasing the free-moving Li^+ concentration.

The high conductivity and 2D structure of MXene help to construct a continuous ion transport network, and reduce the crystallinity of the polymer matrix through interface interaction, thereby significantly improving the ionic conductivity.

MXene can also be used as a mechanical reinforcing phase to improve the mechanical strength of the electrolyte to inhibit lithium dendrite penetration. When MXene is used as a separator functional coating or directly involved in the formation of a solid electrolyte interface, the-F functional group on the surface can promote the formation of a stable SEI layer rich in LiF. This solid and lithium-conducting interface layer can effectively regulate the solvation kinetics of lithium ions, block anion migration, and inhibit interface side reactions, thereby achieving dense and dendrite-free lithium deposition.

8. Summary and Outlooks

Star 2D material MXene has triggered a continuous and extensive research boom in the field of electrochemical energy storage since its discovery due to its unique metal-level conductivity, adjustable surface chemistry, excellent hydrophilicity and mechanical properties. As a battery electrode material, its core value lies primarily in serving as a highly conductive substrate or active material itself, effectively addressing bottlenecks in traditional electrode materials such as poor conductivity, slow ion transport, and significant volume changes. However, transitioning from exceptional performance demonstrations in the laboratory to large-scale commercial application still presents a series of formidable challenges in fundamental science and engineering technology for MXene electrode materials. Future research must not only meet high-performance demands but also navigate increasingly stringent requirements during the strategic transition toward practical implementation. Key focus areas include the following dimensions:

(1) Refinement of energy storage mechanisms. Beyond studying mechanisms involving conductive additives or adsorption sites, the dominant charge storage mechanisms (pseudocapacitive or diffusion-controlled) of MXene in different battery systems, the precise role of functional groups in ion insertion/extraction and catalytic conversion, and the evolution patterns at the electrode/electrolyte interface all require precise clarification using in situ/operating condition characterization techniques and theoretical calculations. Particularly, the microscopic mechanisms underlying structural degradation, functional group loss, and oxidation processes of MXene under high voltage or extreme conditions remain incompletely understood. This is crucial for predicting its lifespan and developing modification strategies;

(2) Eigenvalue optimization. Interlayer stacking issues are invariably encountered during the practical application of 2D sheet materials. Beyond physical approaches, designing appropriate molecular engineering or developing MXene products with intrinsically anti-stacking crystal plane orientations represent effective optimization strategies. Furthermore, activity and stability of MXene can be enhanced through terminal modification engineering (including surface functionalization, atomic doping, or heterojunction formation). This approach facilitates increased active site density and structural robustness while preserving conductivity of MXene;

(3) Process improvements. MXene exhibits exceptional flexibility and film-forming properties, enabling the development of self-supporting films that can be used directly as current collectors in flexible, wearable, and

miniaturized battery systems. However, current MXene preparation methods often involve fluorinated raw materials, posing safety risks and incurring significant environmental costs in subsequent processing. Notably, industrial production demands stringent cost control, making low-cost, safe, environmentally friendly, and efficient manufacturing processes indispensable. Developing fluorine-free/low-fluorine etching routes and mild exfoliation techniques are prerequisites for achieving green, large-scale production;

(4) Integration with machine learning. Artificial intelligence can significantly enhance production efficiency and is currently being deployed on a large scale in scientific research, including in processes such as experimental route design and optimization, as well as material screening [87]. For example, the machine learning model established by Liu 's team based on the experimental results of several MXene cathode materials (Nb_2C, Ti_3C_2, V_2C) successfully predicted the charge-discharge state and initial discharge capacity of Ti_2C cathode in AIBs [88]. Chen's team established a "prediction-driven material design" framework that efficiently identifies optimal structures for MXene-based composites [89]. By integrating robotic automated experiments, active learning sampling, data augmentation, and physical simulations, this approach significantly shortens material development cycles and reduces experimental costs. Consequently, optimal MXene compositions, terminal ratios, composite formulations, and even electrochemical properties can be identified through high-throughput screening or preliminary prediction based on machine learning, greatly accelerating the discovery and optimization of new material systems.

Research on MXene is advancing from fundamental studies to deeper exploration, evolving from simple exfoliated sheets to meticulously designed heterostructures, three-dimensional porous aerogels, and flexible films. Despite ongoing challenges in large-scale synthesis, cost control, and oxidation stability during long-term cycling, the exceptional tunability and multifunctionality of MXene offer precise solutions to address critical bottlenecks in current battery technology development.

Author Contributions

D.G.: conceptualization, methodology, software, data curation, investigation, writing—original draft preparation and editing; X.L.: writing—reviewing, supervision. All authors have read and agreed to the published version of the manuscript.

Funding

This research was funded by the Joint Fund of Henan Province Science and Technology R&D Program (235200810027), Henan Provincial Key R&D and Promotion Special (Science and Technology Tackling) Project (242102230180), Henan Provincial Natural Science Foundation General Project (242300420193), High-level Talent Research Start-up Project Funding of Henan Academy of Sciences (232018002), The Fundamental Research Fund of Henan Academy of Sciences (20250603005), The Scientific and Technological Research Project of Henan Academy of Sciences (20252303002).

Institutional Review Board Statement

Not applicable.

Informed Consent Statement

Not applicable.

Data Availability Statement

The data that support the findings of this study are available from the corresponding author upon reasonable request.

Conflicts of Interest

The authors declare no conflict of interest.

Use of AI and AI-Assisted Technologies

No AI tools were utilized for this paper.

References

1. Nyamathulla, S.; Dhanamjayulu, C. A Review of Battery Energy Storage Systems and Advanced Battery Management System for Different Applications: Challenges and Recommendations. *J. Energy Storage* **2024**, *86*, 111179.
2. Waseem, M.; Ahmad, M.; Parveen, A.; et al. Battery Technologies and Functionality of Battery Management System for EVs: Current Status, Key Challenges, and Future Prospectives. *J. Power Sources* **2023**, *580*, 233349.
3. Hwang, F.S.; Confrey, T.; Reidy, C.; et al. Review of Battery Thermal Management Systems in Electric Vehicles. *Renew. Sust. Energy Rev.* **2024**, *192*, 114171.
4. Naguib, M.; Kurtoglu, M.; Presser, V.; et al. Two-Dimensional Nanocrystals Produced by Exfoliation of Ti_3AlC_2. *Adv. Mater.* **2011**, *23*, 4248–4253.
5. Zhao, L.; Ding, B.; Qin, X.Y.; et al. Revisiting the Roles of Natural Graphite in Ongoing Lithium-Ion Batteries. *Adv. Mater.* **2022**, *34*, 2106704.
6. Wang, H.; Zhao, W.; Guo, Y.; et al. Interlayer Manipulation for Accelerating Ion Diffusion Kinetics in $Ti_3C_2T_x$ MXene Fiber toward Enhanced Supercapacitance with High Rate Capability. *Nano Lett.* **2025**, *25*, 6405–6413.
7. Wang, H.; Cui, Z.; He, S.-A.; et al. Construction of Ultrathin Layered MXene-TiN Heterostructure Enabling Favorable Catalytic Ability for High-Areal-Capacity Lithium-Sulfur Batteries. *Nano Micro Lett.* **2022**, *14*, 189.
8. Chang, L.; Yang, W.; Cai, K.; et al. A Review on Nickel-Rich Nickel-Cobalt-Manganese Ternary Cathode Materials $LiNi_{0.6}Co_{0.2}Mn_{0.2}O_2$ for Lithium-Ion Batteries: Performance Enhancement by Modification. *Mater. Horiz.* **2023**, *10*, 4776–4826.
9. Huang, Y.; Lin, L.; Zhang, C.; et al. Recent Advances and Strategies toward Polysulfides Shuttle Inhibition for High-Performance Li-S Batteries. *Adv. Sci.* **2022**, *9*, 2106004.
10. Li, N.; Xie, Y.; Peng, S.; et al. Ultra-Lightweight $Ti_3C_2T_x$ MXene Modified Separator for Li-S Batteries: Thickness Regulation Enabled Polysulfide Inhibition and Lithium Ion Transportation. *J. Energy Chem.* **2020**, *42*, 116–125.
11. Radjendirane, A.C.; M Sha, F.; Balan, B.; et al. 3D-Polyacrylamide/Ti-MXene: A Newer Hybrid Hydrogel Electrolyte Featuring High Mechanical Strength and Durability for Flexible Aqueous Zinc-Ion Batteries. *ACS Appl. Energy Mater.* **2024**, *7*, 4745–4760.
12. Wang, Z.; Zhang, P.; Zhang, J.; et al. Dendrite-Free Zinc Deposition Enabled by MXene/Nylon Scaffold and Polydopamine Solid-Electrolyte Interphase for Flexible Zinc-Ion Batteries. *Energy Storage Mater.* **2024**, *67*, 103298.
13. Patil, A.M.; You, H.M.; Jadhav, A.A.; et al. Dual Strategies of Na^+ Electrolyte Additives and Dendrites Protective $Ti_3C_2T_x$-MXene/Zn Anode with 2D MXene Nanosheet Encased Niobium Pyrophosphate (NbP_2O_7) Composite Binder-Free Cathode for Stable Zinc-Ion Storage. *Adv. Energy Mater.* **2025**, *15*, 2403322.
14. Xu, H.; Liu, S.; Li, Z.; et al. $Ti_3C_2T_x$ MXene Enhanced PEO/SN-Based Solid Electrolyte for High-Performance Li Metal Battery. *J. Mater. Sci. Technol.* **2025**, *219*, 101–112.
15. Xu, Z.; Huang, H.; Tang, Q.; et al. Coaxially MXene-Confined Solid-State Electrolyte for Flexible High-Rate Lithium Metal Battery. *Nano Energy* **2024**, *122*, 109312.
16. Kumar, D.R.; Karthik, R.; Hasan, M.; et al. Mo-MXene-Filled Gel Polymer Electrolyte for High-Performance Quasi-Solid-State Zinc Metal Batteries. *Chem. Eng. J.* **2023**, *473*, 145207.
17. Xu, H.; Liu, S.; Li, Z.; et al. Synergistic Effect of $Ti_3C_2T_x$ MXene/PAN Nanofiber and LLZTO Particles on High-Performance PEO-Based Solid Electrolyte for Lithium Metal Battery. *J. Colloid Interface Sci.* **2024**, *668*, 634–645.
18. Ma, P.; Fang, D.; Liu, Y.; et al. MXene-Based Materials for Electrochemical Sodium-Ion Storage. *Adv. Sci.* **2021**, *8*, 2003185.
19. Lian, P.; Dong, Y.; Wu, Z.S.; et al. Alkalized Ti_3C_2 MXene Nanoribbons with Expanded Interlayer Spacing for High-Capacity Sodium and Potassium Ion Batteries. *Nano Energy* **2017**, *40*, 1–8.
20. Murali, G.; Reddy Modigunta, J.K.; Park, Y.H.; et al. A Review on MXene Synthesis, Stability, and Photocatalytic Applications. *ACS Nano* **2022**, *16*, 13370–13429.
21. Sabaghi, D.; Polčák, J.; Yang, H.; et al. Multifunctional Molecule-Grafted V_2C MXene as High-Kinetics Potassium-Ion-Intercalation Anodes for Dual-Ion Energy Storage Devices. *Adv. Energy Mater.* **2024**, *14*, 2302961.
22. Li, X.; Huang, Z.; Shuck, C.E.; et al. MXene Chemistry, Electrochemistry and Energy Storage Applications. *Nat. Rev.Chem.* **2022**, *6*, 389–404.
23. Nan, J.; Guo, X.; Xiao, J.; et al. Nanoengineering of 2D MXene-Based Materials for Energy Storage Applications. *Small* **2021**, *17*, 1902085.
24. Ghidiu, M.; Lukatskaya, M.R.; Zhao, M.-Q.; et al. Conductive Two-Dimensional Titanium Carbide 'Clay' with High Volumetric Capacitance. *Nature* **2014**, *516*, 78–81.
25. Lukatskaya, M.R.; Mashtalir, O.; Ren, C.E.; et al. Cation Intercalation and High Volumetric Capacitance of Two-Dimensional Titanium Carbide. *Science* **2013**, *341*, 1502–1505.

26. Yang, C.; Guo, K.; Yuan, D.; et al. Unraveling Reaction Mechanisms of Mo_2C as Cathode Catalyst in a Li-CO_2 Battery. *J. Am. Chem. Soc.* **2020**, *142*, 6983–6990.
27. Zhou, X.; Yu, Z.; Yao, Y.; et al. A High-Efficiency Mo_2C Electrocatalyst Promoting the Polysulfide Redox Kinetics for Na-S Batteries. *Adv. Mater.* **2022**, *34*, 2200479.
28. Zhang, W.; Jin, H.; Du, Y.; et al. Sulfur and Nitrogen Codoped Nb_2C MXene for Dendrite-Free Lithium Metal Battery. *Electrochim. Acta* **2021**, *390*, 138812.
29. Al-Hadeethi, Y.; Iqbal, M.W.; Raffah, B.M.; et al. Synergistic Advancements in Battery-Grade Energy Storage: $Nb_2C/MoTe_2$ (PANI) Hybrid Electrode Material as a Enhanced Electrocatalyst for Hydrogen Reduction Reaction. *Electrochim. Acta* **2024**, *508*, 145205.
30. Guo, W.; She, Z.; Xue, H.; et al. Density Functional Theory Study on the Ti_3CN and Ti_3CNT_2 (T = O, S and F) as High Capacity Anode Material for Na Ion Batteries. *Appl. Surf. Sci.* **2020**, *529*, 147180.
31. Zhang, J.; Zhang, D. Organic-Inorganic Coupled Ti_3CN MXene Achieving the Excellent Sodium-Ion Storage Performance. *Electrochim. Acta* **2024**, *507*, 145102.
32. Tariq, H.A.; Nisar, U.; Abraham, J.J.; et al. TiO_2 Encrusted MXene as a High-Performance Anode Material for Li-Ion Batteries. *Appl. Surf. Sci.* **2022**, *583*, 152441.
33. Byeon, A.; Zhao, M.-Q.; Ren, C.E.; et al. Two-Dimensional Titanium Carbide MXene as a Cathode Material for Hybrid Magnesium/Lithium-Ion Batteries. *ACS Appl. Mater. Interfaces* **2017**, *9*, 4296–4300.
34. Li, X.; Tang, Y.; Liu, L.; et al. Ti_3C_2 MXene with Pillared Structure for Hybrid Magnesium-Lithium Batteries Cathode Material with Long Cycle Life and High Rate Capability. *J. Colloid Interface Sci.* **2022**, *608*, 2455–2462.
35. Li, X.; Ma, X.; Hou, Y.; et al. Intrinsic Voltage Plateau of a Nb_2CT_x MXene Cathode in an Aqueous Electrolyte Induced by High-Voltage Scanning. *Joule* **2021**, *5*, 2993–3005.
36. Zhang, J.; Xia, L.; Yang, L.; et al. $Ti_3C_2T_x$ MXene Nanobelts with Alkali Ion Intercalation: Dual-Purpose for Enhanced Lithium-Ion Batteries and Microwave Absorption. *Carbon* **2025**, *237*, 120148.
37. Li, H.; Meng, R.; Ye, C.; et al. Developing High-Power Li||S Batteries via Transition Metal/Carbon Nanocomposite Electrocatalyst Engineering. *Nat. Nanotechnol.* **2024**, *19*, 792–799.
38. Song, H.; Münch, K.; Liu, X.; et al. All-Solid-State Li-S Batteries with Fast Solid-Solid Sulfur Reaction. *Nature* **2025**, *637*, 846–853.
39. Zhao, Y.; Shang, Z.; Feng, M.; et al. Oriented Assembly of 2D Metal-Pyridylporphyrinic Framework to Regulate the Redox Kinetics in Li-S Batteries. *Adv. Mater.* **2025**, *37*, 2501869.
40. Shi, C.; Zhang, X.; Li, Z.; et al. Review and Perspectives on Preparation Strategies and Applications of Ti_3C_2 MXene for Li Metal Batteries/Li-S Batteries. *Energy Fuels* **2024**, *38*, 14866–14890.
41. Ma, L.; Wang, Y.; Zhu, Z. Interface Engineering of MXene Containing Phosphorus towards for Enhancing the Flame Retardance and Toughness of Epoxy Resins. *Prog. Org. Coat.* **2024**, *191*, 108414.
42. Ranjith, K.S.; Lee, S.-Y.; Ghoreishian, S.M.; et al. Defect and Interface Engineering of MXene-Tagged N, F-Doped Carbon-$CoSe_2$ Heterostructure for Superior Hydrogen Evolution Reactions and Supercapacitors. *Carbon* **2023**, *206*, 246–259.
43. Zaed, M.; Saidur, R.; Pandey, A.; et al. Utilization of Recycled Materials for Low-Cost MXene Synthesis and Fabrication of Graphite/MXene Composite for Enhanced Water Desalination Performance. *Sep. Purif. Technol.* **2025**, *354*, 129055.
44. Wen, J.; Huang, L.; Huang, Y.; et al. A Lithium-MXene Composite Anode with High Specific Capacity and Low Interfacial Resistance for Solid-State Batteries. *Energy Storage Mater.* **2022**, *45*, 934–940.
45. Oliveira, F.M.; Azadmanjiri, J.; Wang, X.; et al. Structure Design and Processing Strategies of MXene-Based Materials for Electromagnetic Interference Shielding. *Small Methods* **2023**, *7*, 2300112.
46. Liu, X.; Zheng, B.; Hua, Y.; et al. Ultralight MXene/rGO Aerogel Frames with Component and Structure Controlled Electromagnetic Wave Absorption by Direct Ink Writing. *Carbon* **2024**, *230*, 119650.
47. Zhang, H.; Li, J.; Luo, L.; et al. Hierarchically Porous MXene Decorated Carbon Coated $LiFePO_4$ as Cathode Material for High-Performance Lithium-Ion Batteries. *J. Alloys Compd.* **2021**, *876*, 160210.
48. Wang, Y.; Lubbers, T.; Xia, R.; et al. Printable Two-Dimensional V_2O_5/MXene Heterostructure Cathode for Lithium-Ion Battery. *J. Electrochem. Soc.* **2021**, *168*, 020507.
49. Wei, C.; Tan, L.; Zhang, Y.; et al. MXene/Organics Heterostructures Enable Ultrastable and High-Rate Lithium/Sodium Batteries. *ACS Appl. Mater. Interfaces* **2022**, *14*, 2979–2988.
50. Zong, H.; Hu, L.; Wang, Z.; et al. Metal-Organic Frameworks-Derived CoP Anchored on MXene toward an Efficient Bifunctional Electrode with Enhanced Lithium Storage. *Chem. Eng. J.* **2021**, *416*, 129102.
51. Zhong, X.; Wang, D.; Sheng, J.; et al. Freestanding and Sandwich MXene-Based Cathode with Suppressed Lithium Polysulfides Shuttle for Flexible Lithium-Sulfur Batteries. *Nano Lett.* **2022**, *22*, 1207–1216.
52. Geng, X.; Liu, C.; Sun, Y.; et al. A $Ti_3C_2T_x$ MXene-Carbon Nanocage-Sulfur Cathode with High Conductivity for Improving the Performance of Li-S Batteries. *J. Alloys Compd.* **2022**, *895*, 162586.

53. Wu, S.; Wang, W.; Shan, J.; et al. Conductive 1T-VS_2-MXene Heterostructured Bidirectional Electrocatalyst Enabling Compact Li-S Batteries with High Volumetric and Areal Capacity. *Energy Storage Mater.* **2022**, *49*, 153–163.
54. Wei, C.; Tian, M.; Fan, Z.; et al. Concurrent Realization of Dendrite-Free Anode and High-Loading Cathode via 3D Printed N-Ti_3C_2 MXene Framework toward Advanced Li-S Full Batteries. *Energy Storage Mater.* **2021**, *41*, 141–151.
55. Zhang, W.; Peng, J.; Hua, W.; et al. Architecting Amorphous Vanadium Oxide/MXene Nanohybrid via Tunable Anodic Oxidation for High-Performance Sodium-Ion Batteries. *Adv. Energy Mater.* **2021**, *11*, 2100757.
56. Xu, E.; Zhang, Y.; Wang, H.; et al. Ultrafast Kinetics Net Electrode Assembled via $MoSe_2$/MXene Heterojunction for High-Performance Sodium-Ion Batteries. *Chem. Eng. J.* **2020**, *385*, 123839.
57. Wang, Z.; Zhang, Y.; Jiang, H.; et al. Free-Standing $Na_2C_6O_6$/MXene Composite Paper for High-Performance Organic Sodium-Ion Batteries. *Nano Res.* **2023**, *16*, 458–465.
58. Zhang, H.; Shen, L.; Geng, X.; et al. MXene-rGO Aerogel Assisted $Na_{3.5}MnTi(PO_4)_3$ Cathode for High-Performance Sodium-Ion Batteries. *Chem. Eng. J.* **2023**, *466*, 143132.
59. Bao, W.; Wang, R.; Qian, C.; et al. Porous Heteroatom-Doped $Ti_3C_2T_x$ MXene Microspheres Enable Strong Adsorption of Sodium Polysulfides for Long-Life Room-Temperature Sodium-Sulfur Batteries. *ACS Nano* **2021**, *15*, 16207–16217.
60. Fang, Y.; Hu, R.; Liu, B.; et al. MXene-Derived TiO_2/Reduced Graphene Oxide Composite with an Enhanced Capacitive Capacity for Li-Ion and K-Ion Batteries. *J. Mater. Chem. A* **2019**, *7*, 5363–5372.
61. Cao, J.; Wang, L.; Li, D.; et al. $Ti_3C_2T_x$ MXene Conductive Layers Supported Bio-Derived $Fe_{x-1}Se_x$/MXene/Carbonaceous Nanoribbons for High-Performance Half/Full Sodium-Ion and Potassium-Ion Batteries. *Adv. Mater.* **2021**, *33*, 2101535.
62. Zhu, J.; Zhang, X.; Gao, H.; et al. VS_4 Anchored on Ti_3C_2 MXene as a High-Performance Cathode Material for Magnesium Ion Battery. *J. Power Sources* **2022**, *518*, 230731.
63. Zhang, Y.; Cao, J.M.; Yuan, Z.; et al. $TiVCT_x$ MXene/Chalcogenide Heterostructure-Based High-Performance Magnesium-Ion Battery as Flexible Integrated Units. *Small* **2022**, *18*, 2202313.
64. Zhu, J.; Shi, R.; Liu, Y.; et al. 3D Interwoven MXene Networks Fabricated by the Assistance of Bacterial Celluloses as High-Performance Cathode Material for Rechargeable Magnesium Battery. *Appl. Surf. Sci.* **2020**, *528*, 146985.
65. Liu, C.; Xu, W.; Mei, C.; et al. Highly Stable $H_2V_3O_8$/Mxene Cathode for Zn-Ion Batteries with Superior Rate Performance and Long Lifespan. *Chem. Eng. J.* **2021**, *405*, 126737.
66. Feng, Y.; Feng, Y.; Zhang, Y.; et al. Flexible Zinc-Ion Microbattery Based on a VS_2/MXene Cathode with High Cycle Life. *J. Power Sources* **2022**, *545*, 231944.
67. Li, M.; Li, X.; Qin, G.; et al. Halogenated Ti_3C_2 MXenes with Electrochemically Active Terminals for High-Performance Zinc Ion Batteries. *ACS Nano* **2021**, *15*, 1077–1085.
68. Zheng, J.; Ju, S.; Yao, L.; et al. Construction of Solid Solution Sulfide Embedded in MXene@N-Doped Carbon Dual Protection Matrix for Advanced Aluminum Ion Batteries. *J. Power Sources* **2021**, *511*, 230450.
69. Lv, W.; Wu, G.; Li, X.; et al. Two-Dimensional V_2C@Se (MXene) Composite Cathode Material for High-Performance Rechargeable Aluminum Batteries. *Energy Storage Mater.* **2022**, *46*, 138–146.
70. Wu, G.; Lv, C.; Lv, W.; et al. Anthraquinone Derivatives Supported by Ti_3C_2 (MXene) as Cathode Materials for Aluminum-Organic Batteries. *J. Energy Chem.* **2022**, *74*, 174–183.
71. Li, J.; Zeng, F.; El-Demellawi, J.K.; et al. Nb_2CT_x MXene Cathode for High-Capacity Rechargeable Aluminum Batteries with Prolonged Cycle Lifetime. *ACS Appl. Mater. Interfaces* **2022**, *14*, 45254–45262.
72. Yuan, Z.; Lin, Q.; Li, Y.; et al. Effects of Multiple Ion Reactions Based on a $CoSe_2$/MXene Cathode in Aluminum-Ion Batteries. *Adv. Mater.* **2023**, *35*, 2211527.
73. Seena, S.; Susanna Victoria Backiyaleela, S.; Sinthika, S.; et al. An Eco-Friendly and Cost-Effective Strategy for the Synthesis of High-Purity MXene. *J. Phys. Chem. C* **2025**, *129*, 8228–8238.
74. Khosla, A.; Sonu; Awan, H.T.A.; et al. Emergence of MXene and MXene-Polymer Hybrid Membranes as Future-Environmental Remediation Strategies. *Adv. Sci.* **2022**, *9*, 2203527.
75. Li, M.; Lu, J.; Luo, K.; et al. Element Replacement Approach by Reaction with Lewis Acidic Molten Salts to Synthesize Nanolaminated MAX Phases and MXenes. *J. Am. Chem. Soc.* **2019**, *141*, 4730–4737.
76. Li, Y.; Shao, H.; Lin, Z.; et al. A General Lewis Acidic Etching Route for Preparing MXenes with Enhanced Electrochemical Performance in Non-Aqueous Electrolyte. *Nat. Mater.* **2020**, *19*, 894–899.
77. Zhang, M.; Liang, R.; Yang, N.; et al. Eutectic Etching toward In-Plane Porosity Manipulation of Cl-Terminated MXene for High-Performance Dual-Ion Battery Anode. *Adv. Energy Mater.* **2022**, *12*, 2102493.
78. Li, X.; Li, M.; Huang, Z.; et al. Activating the I^0/I^+ Redox Couple in an Aqueous I_2-Zn Battery to Achieve a High Voltage Plateau. *Energy Environ. Sci.* **2021**, *14*, 407–413.
79. Wang, Y.; Chen, N.; Zhou, B.; et al. NH_3-Induced *in Situ* Etching Strategy Derived 3D-Interconnected Porous MXene/Carbon Dots Films for High Performance Flexible Supercapacitors. *Nano-Micro Lett.* **2023**, *15*, 231.
80. Chen, C.; Wang, T.; Zhao, X.; et al. Customizing Hydrophilic Terminations for V_2CT_x MXene toward Superior Hybrid-Ion Storage in Aqueous Zinc Batteries. *Adv. Funct. Mater.* **2024**, *34*, 2308508.

81. Liu, F.; Liu, Y.; Zhao, X.; et al. Prelithiated V_2C MXene: A High-Performance Electrode for Hybrid Magnesium/Lithium-Ion Batteries by Ion Cointercalation. *Small* **2020**, *16*, 1906076.
82. Peng, W.; Han, J.; Lu, Y.-R.; et al. A General Strategy for Engineering Single-Metal Sites on 3D Porous N, P Co-Doped $Ti_3C_2T_x$ MXene. *ACS Nano* **2022**, *16*, 4116–4125.
83. Zhao, M.Q.; Xie, X.; Ren, C.E.; et al. Hollow MXene Spheres and 3D Macroporous MXene Frameworks for Na-Ion Storage. *Adv. Mater.* **2017**, *29*, 1702410.
84. Chen, C.; de Kogel, A.; Bikker, L.; et al. Solvation Structure Engineering with Co-Solvents Enables Tunable Charge Storage Mechanisms in MXenes. *Energy Storage Mater.* **2025**, *84*, 104806.
85. He, X.; Xiang, Y.; Yao, W.; et al. MXene Surface Engineering Enabling High-Performance Solid-State Lithium Metal Batteries. *Adv. Funct. Mater.* **2025**, *35*, 2416040.
86. Nomura, Y.; Kawai, K.; Fujita, M.; et al. Real-Time Imaging of Intercalation-Conversion Li Storage in MXenes for Solid-State Batteries. *Small* **2026**, *22*, e13159.
87. Lin, G.; Guo, T.; Lin, W.; et al. Machine Learning Accelerated Screening Advanced Single-Atom Anchored MXenes Electrocatalyst for Nitrogen Fixation. *ACS Catal.* **2025**, *15*, 13534–13548.
88. Li, J.; Xi, S.; Lei, T.; et al. Machine Learning Assisted Prediction in the Discharge Capacities of Novel MXene Cathodes for Aluminum Ion Batteries. *J. Energy Storage* **2024**, *82*, 110196.
89. Yang, H.; Chen, Q.; Chen, T.; et al. Predictive Design of Stretchable Electrodes with Strain-Insensitive Performance via Robotics-and Machine Learning-Integrated Workflow. *Nat. Commun.* **2026**, *17*, 1778.